frontiers | Frontiers in Immunology

TYPE Original Research
PUBLISHED 06 August 2025
DOI 10.3389/fimmu.2025.1624072

OPEN ACCESS

EDITED BY
Nathalie Winter,
Institut National de recherche pour l'agriculture, l'alimentation et l'environnement (INRAE), France

REVIEWED BY
Ana Raquel Maceiras,
Gulbenkian Institute for Molecular Medicine, Portugal
Marina Cella,
Washington University in St. Louis, United States

*CORRESPONDENCE
Shintaro Seto
s-seto@jata.or.jp

RECEIVED 06 May 2025
ACCEPTED 21 July 2025
PUBLISHED 06 August 2025

CITATION
Seto S, Omori S, Nakamura H, Hijikata M and Keicho N (2025) Single-cell transcriptomic profiling reveals a novel signature of necrotizing granulomatous lesions in the lungs of *Mycobacterium tuberculosis*-infected C3HeB/FeJ mice. *Front. Immunol.* 16:1624072. doi: 10.3389/fimmu.2025.1624072

Single-cell transcriptomic profiling reveals a novel signature of necrotizing granulomatous lesions in the lungs of *Mycobacterium tuberculosis*-infected C3HeB/FeJ mice

Shintaro Seto[1*], Shiho Omori[1], Hajime Nakamura[1,2], Minako Hijikata[1] and Naoto Keicho[2,3]

[1]Department of Pathophysiology and Host Defense, The Research Institute of Tuberculosis, Japan Anti-Tuberculosis Association, Tokyo, Japan, [2]Department of Basic Mycobacteriosis, Nagasaki University Graduate School of Biomedical Sciences, Nagasaki, Japan, [3]The Research Institute of Tuberculosis, Japan Anti-Tuberculosis Association, Tokyo, Japan

Tuberculosis (TB) pathology involves complex immune responses within granulomatous lesions. Using single-cell RNA sequencing, we characterized the cellular compositions of necrotizing granulomatous lesions that developed in the lungs of *Mycobacterium tuberculosis*-infected C3HeB/FeJ mice. We identified 11 distinct major cell types, including phagocytes such as neutrophils and macrophages, and T cells, natural killer cells, B cells, dendritic cells, and plasmacytoid dendritic cells. Among T cells, particularly, *Pdcd1*$^{+}$ γδ T cells were detected in necrotizing granulomatous lesions, suggesting their potential role in the pathogenicity of *M. tuberculosis*. Within the macrophage populations, we identified a cluster with significantly higher *Plin2* expression compared to other clusters, whose transcriptomic profile was consistent with that of foamy macrophages. A subset of the *Plin2*-expressing macrophages was identified as a major source of *Ifnb1* and *Cxcl1*, suggesting their involvement in type I interferon signaling and neutrophil recruitment. Furthermore, we identified *Flrt2*, *Hyal1*, and *Mmp13* as novel molecular markers of *Plin2*-expressing macrophages, which were localized to the peripheral rim regions of necrotizing granulomas. In conclusion, our results provide the immune landscape of necrotizing granulomas and reveal novel functional states of macrophages contributing to TB pathogenesis.

KEYWORDS

tuberculosis, *Mycobacterium tuberculosis*, C3HeB/FeJ TB model, necrotizing granuloma, foamy macrophage, scRNA-seq

Introduction

Mycobacterium tuberculosis infects approximately a quarter of the global population and remains the causative agent of tuberculosis (TB), which is one of the leading causes of death worldwide (1). Over a lifetime, 5–10% of infected individuals eventually develop active TB disease. Understanding the immunological conditions leading to TB progression is crucial for the development of new vaccines, early diagnostics, and host-directed therapies.

Upon inhalation, *M. tuberculosis* bacilli are phagocytosed by alveolar macrophages, followed by their migration into the interstitial space in the lungs (2). Due to their inability to control the intracellular replication of *M. tuberculosis* (3), infected macrophages secrete cytokines and chemokines that recruit lymphocytes and additional macrophages from blood vessels. The resulting aggregation of immune cells leads to the formation of granulomas (4). Despite the heterogeneity of granulomatous lesions, necrotizing granulomas are a pathological hallmark in TB patients (5–7). Moreover, foamy macrophages play critical roles in granuloma formation, development, maintenance, and dissemination of infection (5, 8). These foamy macrophages serve as a niche for *M. tuberculosis* replication (9), and their cell death is believed to contribute to the formation of necrotic cores within granulomas (5, 8).

Recent studies on TB pathology have focused on the cellular heterogeneity of granulomas by analyzing their cellular composition and transcriptomic profiles. Advanced technologies such as single-cell RNA sequencing (scRNA-seq) and spatial transcriptomics have been applied to lung tissues from TB patients, and *M. tuberculosis*-infected non-human primates and mice (10–28). Although transcriptomic analyses combined with laser microdissection have revealed significantly elevated *Plin2* expression in foamy macrophages within necrotizing granulomas in the lungs of both TB patients and C3HeB/FeJ mice (29, 30), single-cell transcriptomic profiling specifically targeting foamy macrophages remains limited.

In this study, we employed a TB mouse model using C3HeB/FeJ mice, which develop necrotizing granulomas upon *M. tuberculosis* infection and closely recapitulate the pathological features observed in human TB (7). Using scRNA-seq, we characterized the cellular composition and transcriptomic profiles of necrotizing granulomatous lesions in the lungs of this mouse model. The findings of this study will reveal unique transcriptional signatures of foamy macrophages, highlighting their potential as targets for novel TB diagnostics and host-directed therapeutics.

Results

Single cell transcriptomics reveals the cellular landscape of necrotizing granulomatous lesions

C3HeB/FeJ mice infected with *M. tuberculosis* via aerosol exposure developed necrotizing granulomatous lesions in the lungs at 12 weeks postinfection (p.i.) (Supplementary Figure 1), which is consistent with previous reports (30–34). We collected lung lesions with necrotic granulomas and prepared single-cell suspensions. To optimize the resolution of cellular transcriptomics, cell suspensions were further separated using Ficoll-Paque density gradient centrifugation, as necrotizing granulomas are primarily composed of abundant neutrophils and dead cell debris (30, 33, 35, 36). Cells collected from the interface layers of Ficoll-Paque solution were subjected to scRNA-seq (Figures 1A, B). Among 30,159 cells isolated from necrotizing granulomatous lesions, we manually annotated 11 major cell types. These included phagocytotic cells such as neutrophils and macrophages; dendritic cells (DCs)

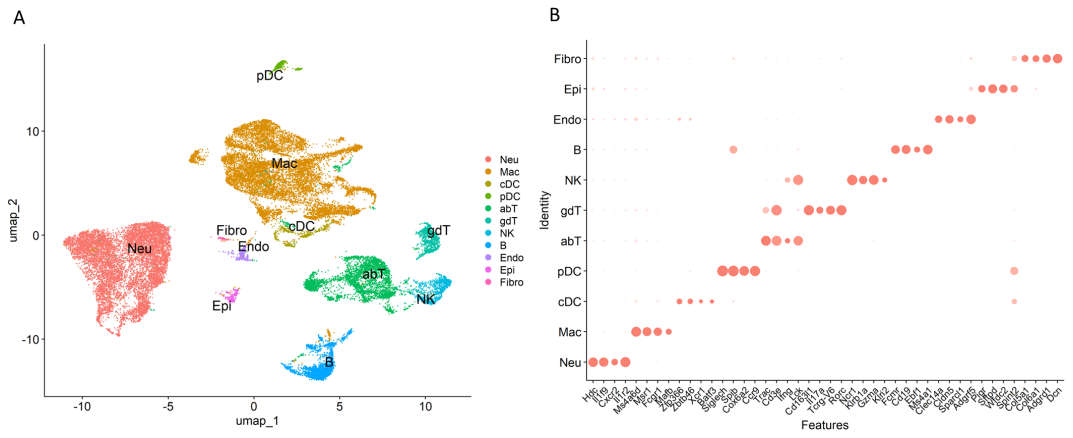

FIGURE 1
Single-cell transcriptomic landscape of necrotizing granulomatous lesions developed in *Mycobacterium tuberculosis*-infected lungs of C3HeB/FeJ mice. **(A)** Uniform manifold approximation and projection (UMAP) plot of 30,159 cells isolated from necrotizing granulomas, showing 11 major cell types. Neu, neutrophil; Mac, macrophage, cDC, conventional dendritic cell; pDC, plasmacytoid DC; abT, αβ T cell; gdT, γδ T cell; NK, natural killer cell; B, B cell; Endo, endothelial cell, Epi, epithelial cell, Fibro, fibroblast. **(B)** Dot plot showing the distinct expression of selected marker genes in each cell cluster.

including conventional DCs (cDCs) and plasmacytoid DCs (pDCs); T cells including αβ T cell and γδ T cell subsets; natural killer (NK) cells; and B cells.

Assessment of T cell populations in necrotizing granulomas lesions

Next, we assessed the subclusters of T cells within the necrotizing granulomatous lesions (Figure 2, Supplementary Figure 2). Among $CD4^+$ T cells, three clusters were identified: effector T cells, naïve T cells, and regulatory T cells (Tregs). For $CD8^+$ T cells, two clusters were observed: cytotoxic and exhausted $CD8^+$ T cells. Furthermore, we identified tissue-resident memory T cells (TRM) either expressing CD4 or CD8 within necrotizing granulomas.

During *M. tuberculosis* infection, γδ T cells participate in the immune response in the lungs (37). In particular, IL-17-mediated immunity is critical for γδ T cells to perform their function in host defense in TB murine models (38). In necrotizing granulomas, γδ T cells expressing *Il17a* were identified (Figures 2C, D). These γδ T cells also expressed *Pdcd1*, which encodes programmed cell death-1 (PD-1), an immune checkpoint molecule inhibiting immune responses (39).

Among other T cell types, we identified a unique population co-expressing *Tcrg* (T cell receptor gamma) and *Klrd1* (encoding an NK cell receptor) (Figures 2B, C). This population also expressed *Gata3*, *Tbx21*, *Il7r*, *Cd7*, and *Xcl1* (Supplementary Figures 2A, C), suggesting the presence of certain innate lymphoid cells (ILCs) expressing these markers.

Following the removal of doublet cells from the scRNA-seq data, we observed clusters expressing both T cell markers (such as CD3e) and characteristic genes of neutrophils or macrophages (Figure 2B, Supplementary Figure 2C). This observation may reflect biological processes such as the phagocytosis of T cell-derived material; however, further analyses are required to confirm this phenomenon.

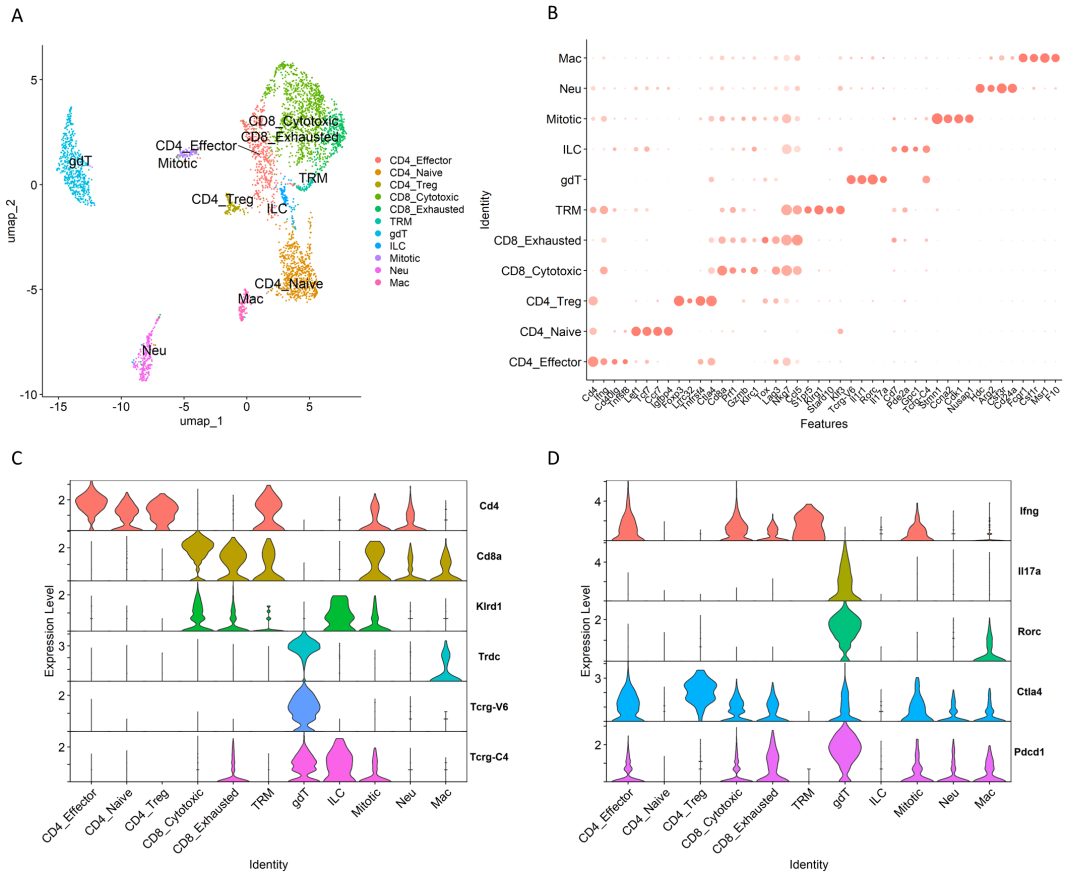

FIGURE 2
T cell clusters within necrotizing granulomatous lesions. T cell populations from necrotizing granulomas were further filtered to remove doubles and subsequently re-clustered. **(A)** UMAP plot showing T cell populations, including αβ T cells and γδ T cells. CD4_Effector, effector $CD4^+$ T cell; CD4_Naive, naïve $CD4^+$ T cell; CD4_Treg, regulatory $CD4^+$ T cell; CD8_Cytotoxic, cytotoxic $CD8^+$ T cell, CD8_exhausted, exhausted $CD8^+$ T cell; TRM, tissue-resident memory T cell; gdT, γδ T cell; ILC, innate lymphoid cell; Mitotic, mitotic cell; Neu, neutrophil; Mac, macrophage. **(B)** Dot plot displaying the expression of selected marker genes for identified T cell clusters. **(C, D)** Violin plots displaying gene expression levels of T cell receptors and co-receptor molecules **(C)** and cytokines and immune checkpoint molecules **(D)**.

Macrophage populations in necrotizing granulomatous lesions

To investigate the hallmark of macrophage populations within necrotizing granulomas, we analyzed their gene expression profiles. Given that *Plin2* expression is significantly upregulated in foamy macrophages within necrotizing granulomas (29, 30), we identified the cluster exhibiting significantly elevated *Plin2* expression compared to other clusters (Figure 3A). To characterize the remaining clusters, we analyzed their gene expression profiles and found that macrophages expressing *Cxcl10*, *Clec4e*, *C1qc*, *Ighm*, *S100a9*, or *Siglecf* also represented distinct macrophage populations within the necrotizing granulomatous lesions (Figure 3A). Moreover, we confirmed that the expression levels of the

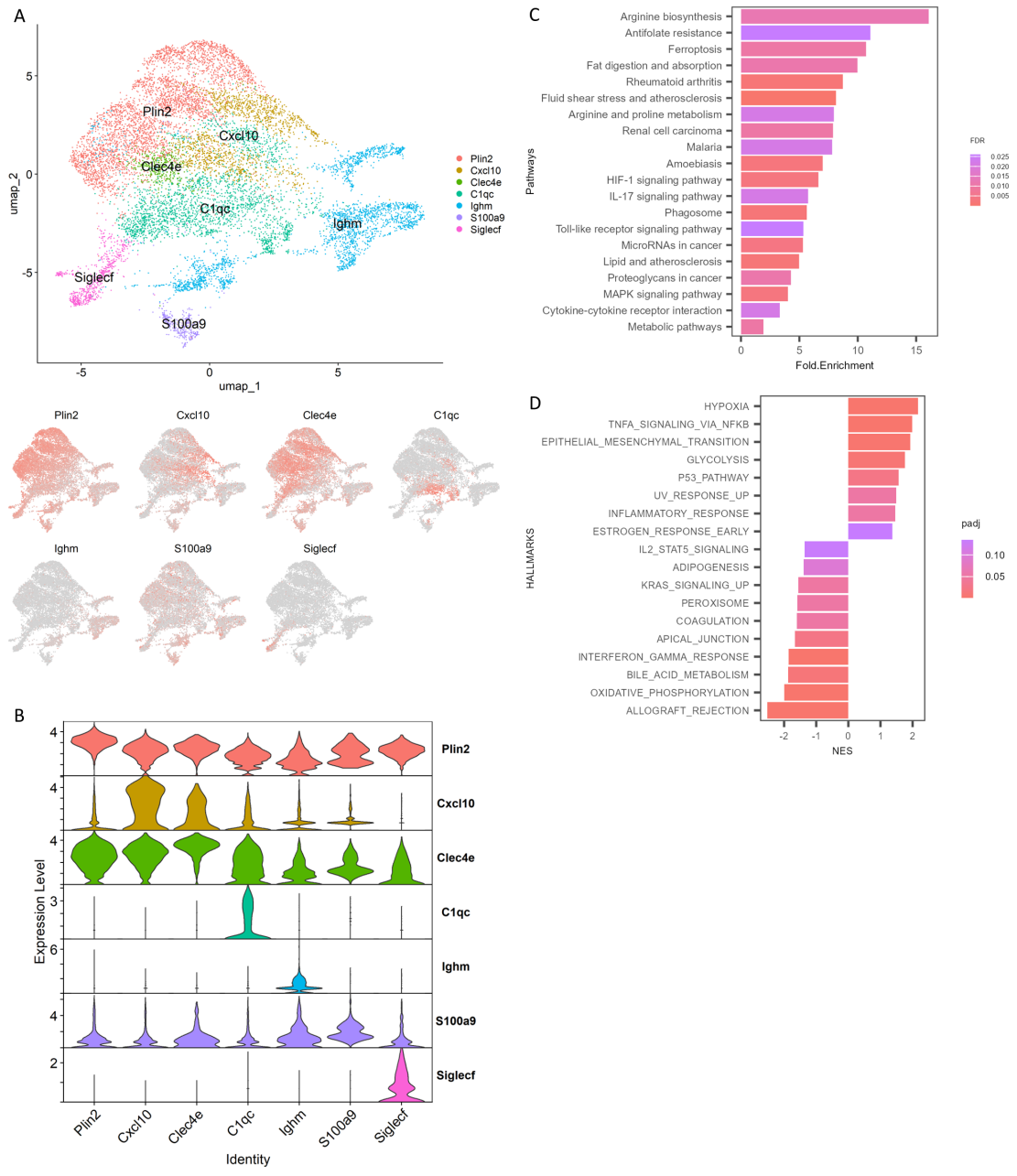

FIGURE 3
Identification of foamy macrophage associated subclusters. Macrophage populations in necrotizing granulomas were re-clustered and analyzed. **(A)** UMAP plot of macrophage clusters in necrotizing granulomatous lesions, characterized by signature genes. The expression patterns of signature genes are also depicted. **(B)** Violin plot showing significantly elevated expression of the indicated genes in specific clusters. **(C)** Bar plot showing gene ontology analysis of differentially expressed genes upregulated in the *Plin2*-expressing macrophage cluster. Top 20 enriched KEGG pathways are indicated, along with fold of enrichment (Fold.Enrichment) and false discovery rate (FDR). **(D)** Gene set enrichment analysis (GSEA) of *Plin2*-expressing macrophage cluster. Significantly enriched hallmarks are depicted, representing both activated and suppressed hallmarks in the *Plin2*+ cluster compared with other clusters.

corresponding genes in their respective clusters were significantly higher than those in other clusters (Figure 3B).

We investigated the differentially expressed genes between the *Plin2*-expressing (*Plin2*$^+$) cluster and other clusters within the macrophage population. Genes that were significantly upregulated in the *Plin2*$^+$ cluster were selected (Supplementary Table 1) and subjected to Gene Ontology (GO) enrichment analysis (Figure 3C). Genes related to fat digestion and absorption, as well as lipid and atherosclerosis, were found to be upregulated. To further investigate the gene expression profile of *Plin2*$^+$ cluster, we performed gene set enrichment analysis (GSEA) (Figure 3D). GSEA revealed that genes associated with hypoxia, TNF-α signaling, glycolysis, and inflammatory responses were upregulated, whereas those associated with oxidative phosphorylation and type II interferon (IFN) responses were downregulated in the *Plin2*$^+$ cluster compared to other macrophage clusters.

We investigated the gene expression profiles of additional macrophage clusters within necrotizing granulomatous lesions using GSEA (Supplementary Figure 3). Clusters expressing *Cxcl10 or Clec4e* exhibited gene expression signatures characteristic of pro-inflammatory macrophages. In contrast, clusters expressing *C1qc*, *Ighm*, or *Siglecf* showed gene expression profiles associated with anti-inflammatory macrophages. A more detailed analysis revealed that *Ighm*$^+$ macrophages expressed several anti-inflammatory genes, including *Cd244a*, *Nr4a1*, *Clec4a1*, and *Clec4a2* (Supplementary Figure 4A). Since *Siglecf* is a well-established marker of alveolar macrophages (40), the *Siglecf*$^+$ cluster was identified as alveolar macrophages. *Siglecf*-expressing macrophages expressed *Alox5*, a gene that promotes anti-inflammatory polarization and contributes to increased susceptibility to *M. tuberculosis* infection (41, 42) (Supplementary Figure 4B). Trem2 has been shown to act as a receptor for mycolic acid from mycobacteria and to limit anti-mycobacterial macrophage activation (43). The expression of *Trem2* was mainly observed in the *Siglecf*$^+$ cluster (Supplementary Figure 4B). These results suggest that macrophages in the *Siglecf*$^+$ cluster may contribute to a permissive environment for *M. tuberculosis* infection within necrotizing granulomatous lesions.

Novel polarization of *Plin2*-expressing macrophages

Nos2 and *Arg1*, well-established markers of macrophage polarization, play key roles in regulating immune responses (44, 45). We have previously demonstrated that Plin2-expressing macrophages express Nos2 or Arg1 in necrotizing granulomas (30), suggesting that the polarization of foamy macrophages exhibits either pro-inflammatory or anti-inflammatory characteristics. Accordingly, scRNA-seq profiling revealed that *Nos2* was highly expressed in pro-inflammatory macrophage clusters including the *Plin2*$^+$ cluster (Figure 4A). Moreover, *Arg1* expression was predominantly observed in the *Plin2*$^+$ cluster. Feature plots revealed the presence of *Plin2*$^+$ macrophages co-expressing *Nos2* and *Arg1* (Figure 4B). Further, we investigated the transcriptional factors associated with the regulation of *Nos2* or *Arg1* expression in macrophages within necrotizing granulomas. Among them, we found that *Irf7* expression was correlated with *Nos2* expression patterns in macrophage clusters (Figure 4A). *Irf7* regulates macrophage polarization toward both pro-inflammatory and anti-inflammatory states (46). *Fosl1* encodes a transcription factor that promotes pro-inflammatory polarization by repressing *Arg1* expression (47). We observed *Fosl1* expression in a subset of *Arg1*$^+$ macrophages within the *Plin2*$^+$ cluster (Figure 4C), suggesting that *Plin2*$^+$ macrophages may consist of heterogeneous subpopulations with distinct or transitional polarization states. These findings suggest that *Irf7* and *Fosl1* may contribute to the dynamic regulation of macrophage polarization within necrotizing granulomas.

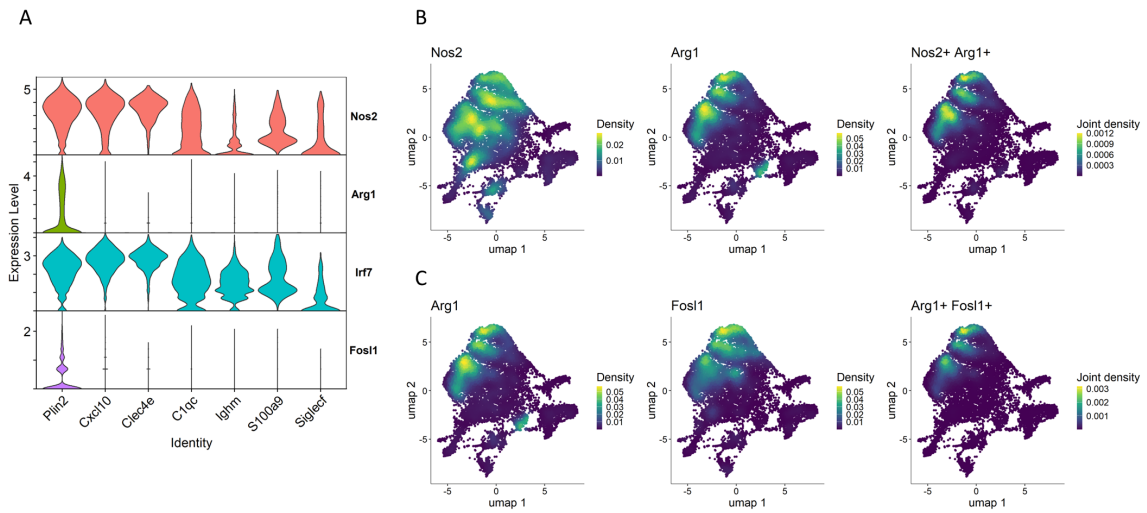

FIGURE 4
Novel polarization of the *Plin2*$^+$ macrophage cluster. **(A)** Violin plots showing the gene expression of *Nos2* and *Arg1* and their transcriptional factors *Irf7* and *Fosl1* in macrophage clusters. **(B)** UMAP plot illustrating expression and co-expression of *Nos2* and *Arg1* in macrophages. **(C)** Expression and co-expression of *Arg1* and *Fosl1* in macrophages.

We further analyzed polarization states of macrophages derived from myeloid cell lineages in the whole lungs of *M. tuberculosis*-infected *Sp140* knockout (KO) mice, using the data from Kotov et al. (28). In C3HeB/FeJ mice, the reduced gene expression of both *Sp110* and *Sp140* in *Sst1* locus contributes to increased susceptibility to *M. tuberculosis* infection (48–50). In addition, similar to C3HeB/FeJ mice, *Sp140* KO mice also exhibit increased susceptibility to *M. tuberculosis* infection, indicating that *Sp140* is a key determinant of host vulnerability to the infection (51). Macrophage populations derived from *M. tuberculosis*-infected *Sp140* KO mice were re-clustered based on the original annotations (Figure 5A). Subsequently, *Plin2* expression was found to be elevated in the cluster of interferon-stimulated gene-positive (ISG^+) interstitial macrophages (IMs) compared to other macrophage clusters. This result suggests that ISG^+ IMs correspond to the $Plin2^+$ cluster identified in our study (Figure 5B). This was further supported by a comparative analysis of macrophage populations between C3HeB/FeJ mice and *Sp140* KO mice (Supplementary Figures 5A, B). Notably, *Nos2* was expressed in ISG^+ IM and IM populations, whereas *Arg1* was dominantly expressed in $ISGs^+$ IMs (Figure 5B, Supplementary Figure 5C). Moreover, macrophages co-expressing *Nos2* and *Arg1* were observed in a subset of the ISG^+ IM cluster (Figure 5C). These results suggest the emergency of a novel macrophage polarization state in ISG $^+$ IMs derived from *M. tuberculosis*-infected *Sp140* KO mice, corresponding to the $Plin2^+$ cluster of C3HeB/FeJ mice identified in our study.

Gene expression characteristic of *Plin2*-expressing macrophages

Type I IFNs and neutrophils contribute to TB exacerbation (35, 52). Accordingly, we investigated the expression of *Ifnb1*, a type I IFN gene, and *Cxcl1*, a chemokine gene involved in neutrophil recruitment, in macrophage populations (Figure 6). Both genes were specifically expressed in the $Plin2^+$ cluster, consistent with previous reports (28, 35).

We investigated novel gene expression signatures characteristic of the $Plin2^+$ cluster within necrotizing granulomas. Among the genes expressed in the $Plin2^+$ cluster, *Flrt2*, *Hyal1*, and *Mmp13* were selected for further examination, due to their specific and enriched expression patterns (Figures 7A, B). IHC revealed that these proteins were localized to the rim regions of necrotizing granulomas, consistent with Plin2 localization (Figure 7C). Immunofluorescence microscopy

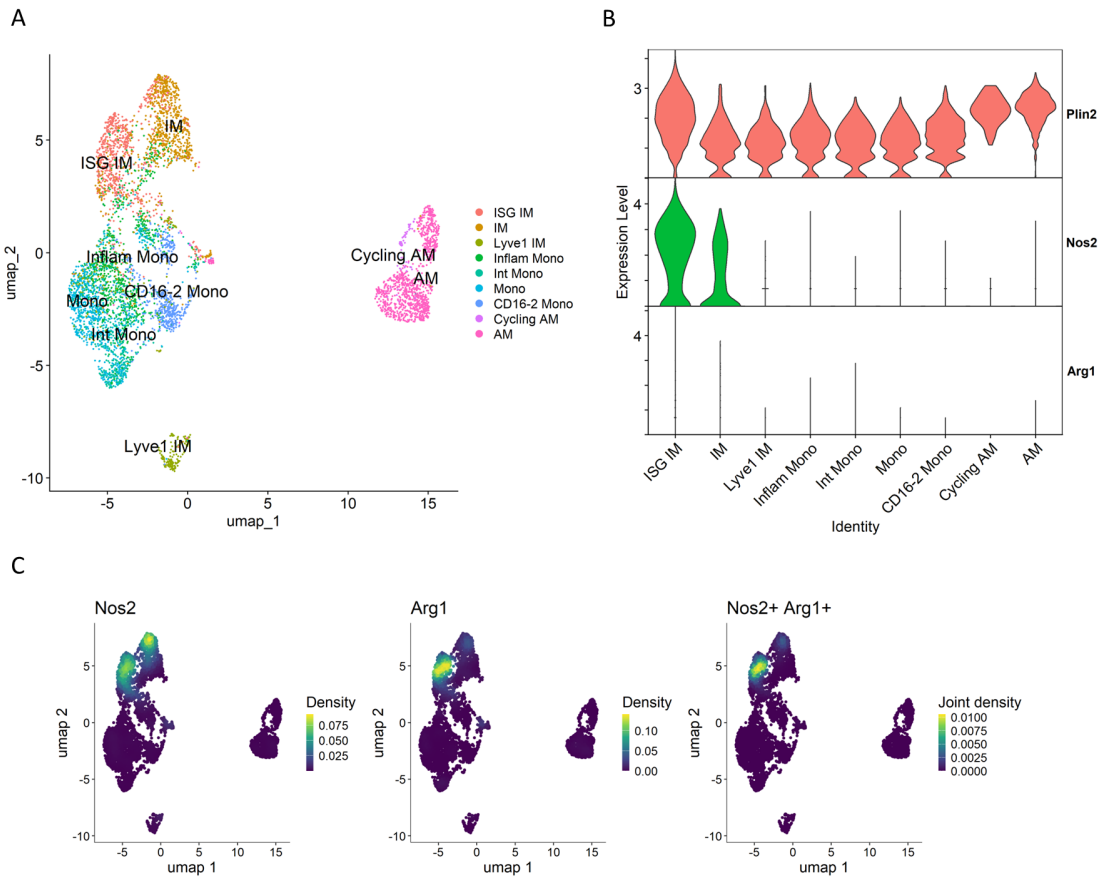

FIGURE 5
Macrophages derived from *M. tuberculosis*-infected *Sp140*-deficient mouse lungs. Macrophage populations of the GSE216023 data from Kotov et al. (28) were analyzed. **(A)** UMAP plot of macrophage populations from *Sp140* knockout (KO) mouse lungs infected with *M. tuberculosis*. **(B)** Volin plot showing expression levels of *Plin2*, *Nos2* and *Arg1* in macrophage clusters derived from *Sp140* KO mice. **(C)** UMAP plot showing expression and co-expression of *Nos2* and *Arg1* in macrophages derived from *Sp140* KO mice.

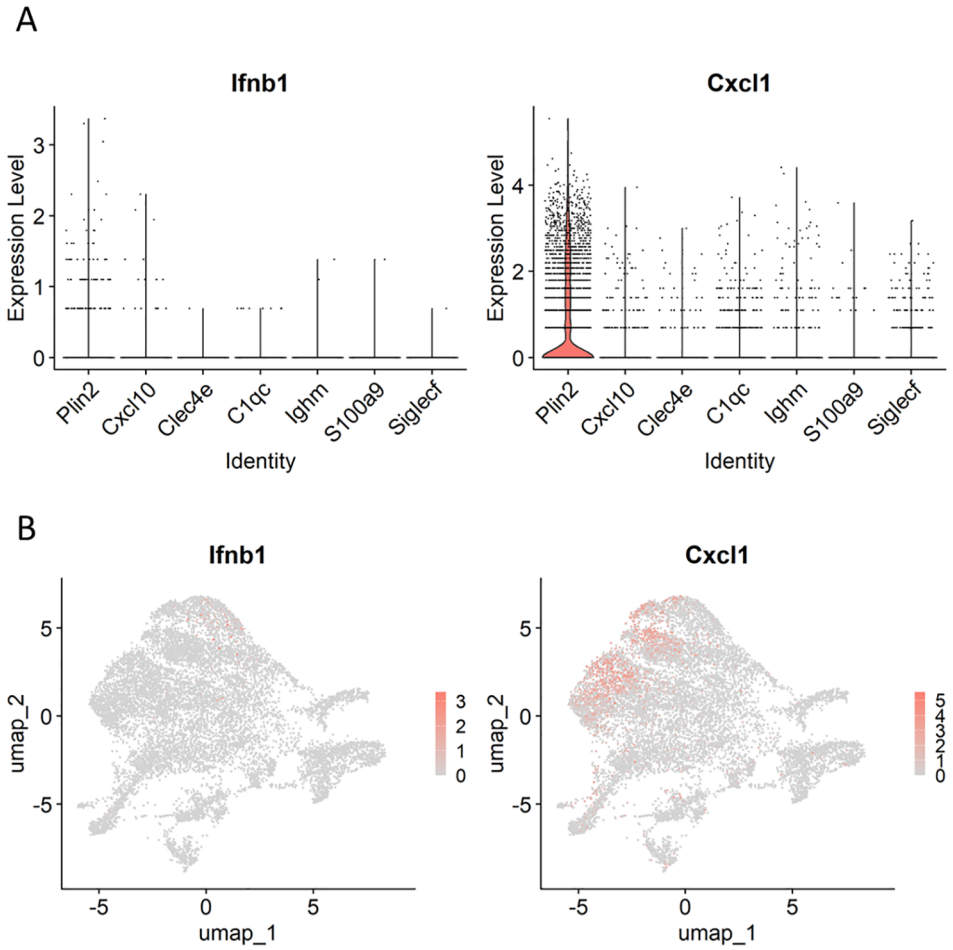

FIGURE 6
Expression profiles of genes involved in tuberculosis (TB) exacerbation in macrophages. Violin **(A)** and UMAP **(B)** plots demonstrating *Ifnb1* and *Cxcl1* expression in macrophage clusters.

(IFM) showed co-localization of all the three proteins with Plin2$^+$ cells. Notably, the fluorescent signals of Flrt2, Hyal1, and Mmp13 displayed distinct subcellular localization patterns, whereas Plin2 was predominantly localized to the cytosolic regions of the same vacuolated cells (Figure 7D). These results suggest that *Flrt2*, *Hyal1*, and *Mmp13* are novel molecular markers characterizing *Plin2*$^+$ macrophages in necrotizing granulomas.

pDC expressed immunomodulatory and cytotoxic factors in necrotizing granulomatous lesions

pDCs regulate viral infections by producing a large amount of type I IFNs (53). In the context of *M. tuberculosis* infection, the depletion of pDCs results in increased bacterial burdens in the lungs (28). Lee et al. demonstrated that *M. tuberculosis*-infected neutrophils can stimulate pDCs to produce type I IFNs (54). Therefore, we assessed the expression levels of *Ifnb1* in pDCs (Figures 8A, B). However, *Ifnb1* expression were predominantly detected in macrophages rather than pDCs. In contrast, pDCs expressed *Il34* and *Kmo*. *Il34* encodes an anti-inflammatory cytokine that regulates the expression of pro-inflammatory cytokines and promotes macrophage polarization toward an anti-inflammatory phenotype (55). *Kmo* encodes kynurenine 3-monooxygenase, which catalyzes the conversion of kynurenine to 3-hydroxykynurenine (3-HK), a metabolite inducing cellular damage and apoptosis via oxidative stress (56). These results suggest that pDCs are localized to necrotizing granulomatous lesions and contribute to the pathogenicity of *M. tuberculosis* infection via the expression of immunomodulatory and cytotoxic factors.

Discussion

scRNA-seq has been widely utilized to evaluate the cellular transcriptomics of tissues or blood samples from TB patients, as well as from *M. tuberculosis*-infected non-human primates, mice and other experimental models (57). However, the detailed cellular composition of necrotizing granulomatous lesions, a hallmark of TB pathology (5, 7), remains incompletely characterized. In this study,

10.3389/fimmu.2025.1624072

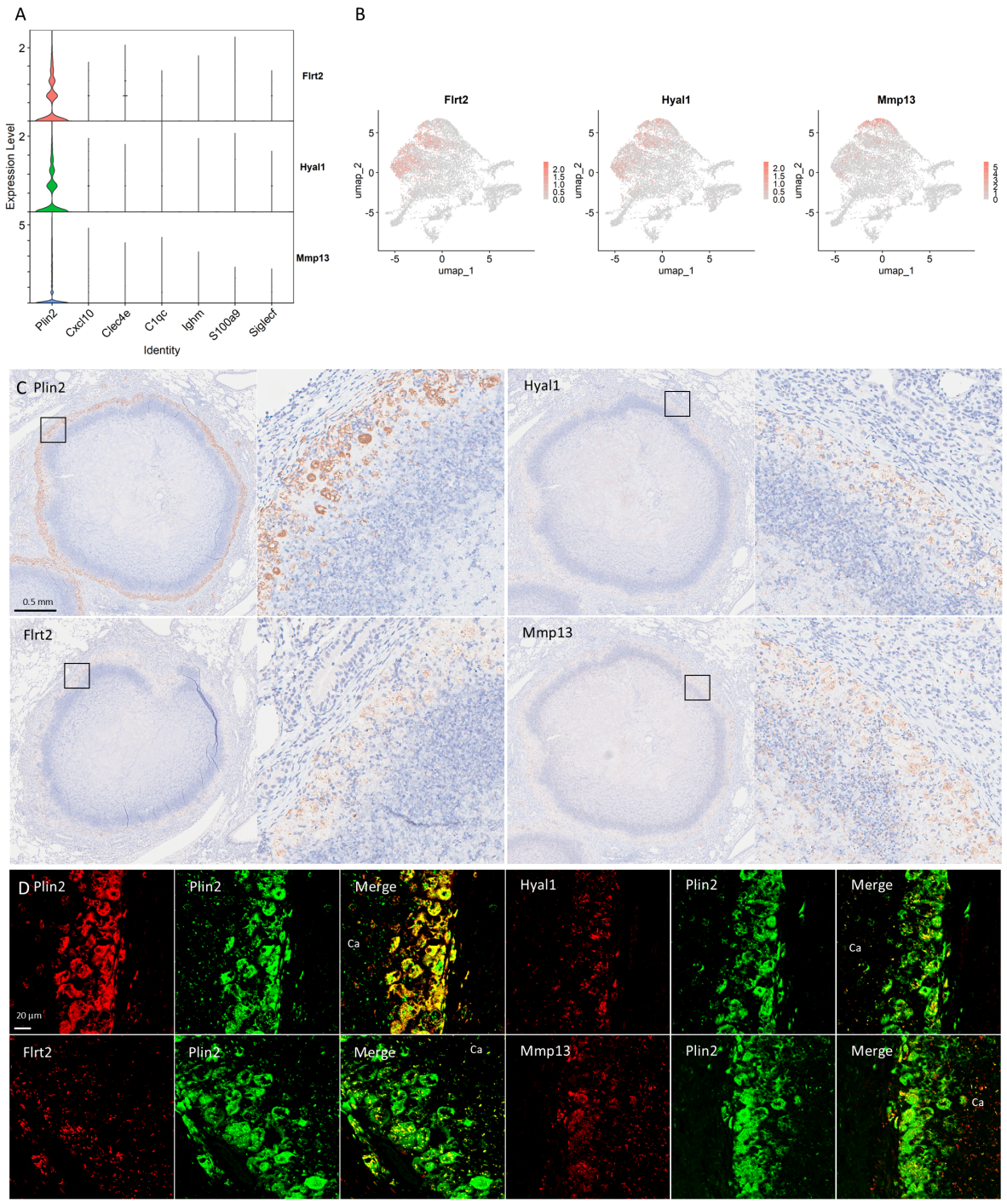

FIGURE 7
Novel signature of foamy macrophages in necrotizing granulomas. **(A)** Violin plots demonstrating the expression of *Flrt2*, *Hyal1*, and *Mmp13*, specifically expressed in the *Plin2*+ cluster. **(B)** UMAP plots demonstrating the expression of *Flrt2*, *Hyal1*, and *Mmp13*, specifically associated with the *Plin2*$^{+}$ cluster. **(C)** Immunohistochemistry images showing the localization of Flrt2, Hyal1, and Mmp13 in necrotizing granulomas. The marker for foamy macrophages, Plin2 is also shown. For each protein localization, the right panel displays an enlarged view of the area indicated by a square in the corresponding left panel. **(D)** Immunofluorescence microscopic images demonstrating co-localization of Plin2 with the indicated proteins in necrotizing granulomas. Ca, caseous necrosis region within necrotizing granulomas.

we isolated single-cell suspensions from necrotizing granulomatous lesions developed in the lungs of *M. tuberculosis*-infected C3HeB/FeJ mice, and performed scRNA-seq to comprehensively investigate their cellular landscape. We identified 11 major cell type, including immune cells such as neutrophils, macrophages, dendritic cells, T cells, NK cell, and B cells (Figure 1). To prepare single-cell suspensions from necrotizing granulomatous lesions, we performed Ficoll-Paque density gradient centrifugation to reduce

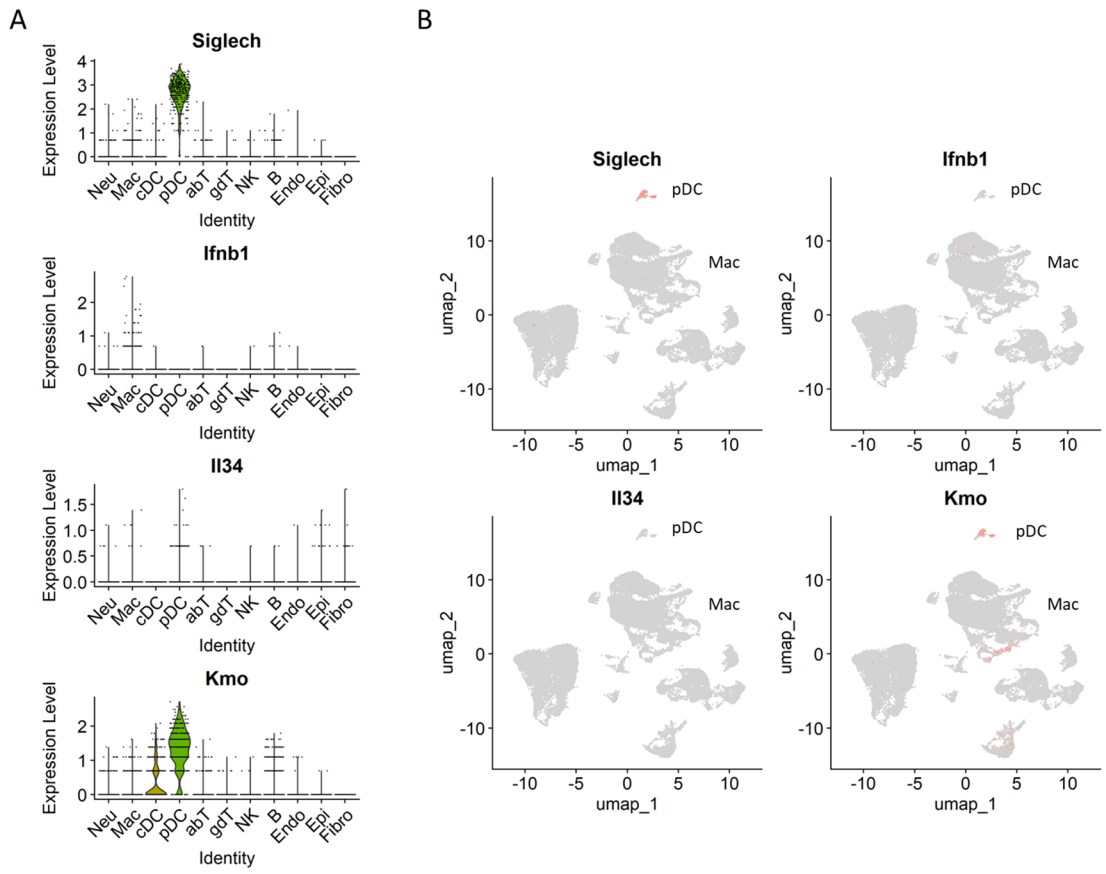

FIGURE 8
Expression of *Il34* and *Kmo* in necrotizing granulomas of *M. tuberculosis*-infected C3HeB/FeJ mice. Violin **(A)** and UMAP **(B)** plots showing the gene expression of *Ifnb1*, *Il34*, *Kmo* and *Siglech* (pDC marker) in necrotizing granulomas derived from *M. tuberculosis*-infected C3HeB/FeJ mice.

the number of dead cells and neutrophils. However, due to the heterogeneity and activation states of neutrophils, their density can vary, resulting in partial retention at the interface of the Ficoll-Paque gradient.

Among T cells, $CD4^+$ T cells, particularly central memory *Mtb*-specific $CD4^+$ T cells, play a crucial role in protective immunity against *Mtb* infection (58). In this study, we identified $CD4^+$ T cells in necrotizing granulomatous lesions as naïve, effector or TRM types (Figure 2, Supplementary Figure 2). However, central memory $CD4^+$ T cells ($Cd44^+$, $Sell^+$, and $Ccr7^+$) were not identified, suggesting that these cells do not localize to necrotizing granulomatous lesions. Naïve $CD4^+$ T cells were enriched in the lesions, consistent with previous reports in non-human primate and murine models of *M. tuberculosis* infection (25–27). Moreover, $Pdcd1^+$ γδ T cells were identified within necrotizing granulomatous lesions (Figure 2). Although IL-17-producing γδ T cells play a protective role in the lungs of *M. tuberculosis*-infected mice (59), the presence of $Pdcd1^+$ γδ T cells has not been previously reported in this context. In the experimental autoimmune encephalomyelitis mouse model, $Pdcd1^+$ γδ T cells have been implicated in promoting disease pathogenesis (60). These findings suggest that $Pdcd1^+$ γδ T cells may similarly contribute to the immunopathology of necrotizing granulomas during *M. tuberculosis* infection.

In macrophage populations within necrotizing granulomas, the $Plin2^+$ cluster was identified based on *Plin2* expression in the clusters (Figure 3). Because Plin2 is the marker of foamy macrophages in the lungs of TB patients and *M. tuberculosis*-infected C3HeB/FeJ mice (29, 30), we referred to the $Plin2^+$ cluster as the foamy macrophage population. Furthermore, differential gene expression analysis and GSEA revealed that gene expression profiles of the $Plin2^+$ cluster were consistent with the characteristics of foamy macrophages in necrotizing granulomas (29, 30).

Previously, we have demonstrated that foamy macrophages in necrotizing granulomas express typical macrophage polarization markers, either *Nos2* or *Arg1*, suggesting their differentiation into a pro-inflammatory or anti-inflammatory state (30). scRNA-seq revealed that $Plin2^+$ macrophages express *Nos2* or *Arg1* (Figure 4). Moreover, we identified a subset of $Plin2^+$ macrophages co-expressing both *Nos2* and *Arg1*, suggesting a novel polarization state of foamy macrophages in necrotizing granulomas. A similar polarization profile was also observed in macrophage populations isolated from the lungs of *M. tuberculosis*-infected *Sp140* KO mice (28) (Figure 5). Foamy macrophages exhibiting the dual expression profile may represent a transitional state between pro- and anti-inflammatory phenotypes. To investigate this possibility, we performed a comparative analysis of

macrophage populations between C3HeB/FeJ and *Sp140* KO mice (Supplementary Figure 5). This analysis revealed a distinct correspondence between the *Plin2*$^+$ cluster in C3HeB/FeJ mice and ISG$^+$ IMs in *Sp140* KO mice, as well as between the *C1qc*+ cluster and IMs, the *Ighm*+ cluster and monocyte clusters, the *Siglecf*$^+$ cluster and alveolar macrophage clusters. Together, these results suggest that monocytes infiltrating infected lungs differentiate into IMs and ISG$^+$ IMs, subsets of which further progress toward a foamy macrophage phenotype.

Type I IFNs and neutrophils are key exacerbating factors in TB, contributing to disease progression by promoting inflammation and inducing the release of neutrophil extracellular traps (NETs) (35, 51, 52). In particular, neutrophils and their remnants resulting from NETosis accumulate in the caseous necrosis regions of necrotizing granulomas. We found a subset of *Plin2*$^+$ macrophages expressing *Ifnb1* or *Cxcl1* (Figure 6). scRNA-seq revealed that ISG$^+$ IMs and IMs express type I IFNs in the lungs of *M. tuberculosis*-infected *Sp140* KO mice (28). Chowdhury et al. demonstrated that type I IFNs are primarily expressed by epithelioid cells proximal to the caseous necrosis regions in necrotizing granulomas developed in C3HeB/FeJ mice and non-human primate models (35), which is consistent with our findings. Moreover, Chowdhury et al. demonstrated that pDCs within necrotizing granulomatous lesions are not significantly associated with type I IFN expression. In agreement with this, our study revealed that pDCs within necrotizing granulomatous lesions do not predominantly express *Ifnb1*, but rather express other immunosuppressive genes, such as *Il34* and *Kmo* (Figure 8). These results suggest that Cxcl1, secreted by foamy macrophages in necrotizing granulomas, contribute to the recruitment of neutrophils into the caseous necrosis regions, where NETosis may be subsequently induced by type I IFNs.

We investigated unique molecular signatures of the *Plin2*+ cluster in necrotizing granulomas. We found that three proteins, Flrt2, Hyal1, and Mmp13, were specifically localized to Plin2$^+$ macrophages (Figure 7). *Flrt2* regulates macrophage differentiation and activate Akt/mTOR signaling (61). Given the involvement of mTORC1 signaling in the differentiation of foamy macrophages during *M. tuberculosis* infection (62), *Flrt2* may contribute to foamy macrophage differentiation in necrotizing granulomas. *Hyal1* encodes a lysosomal hyaluronidase that digests extracellular matrix (63). We found that a subset of *Cxcl1*-expressing *Plin2*$^+$ macrophages also expressed *Hyal1* (Supplementary Figure 4C), suggesting that *Hyal1* facilitates neutrophil recruitment into the caseous necrosis regions. *Mmp13* encodes a metalloprotease involved in collagen remodeling in atherosclerotic plaques (64). Foamy macrophages exhibit a characteristic arrangement around the necrotic core within necrotizing granulomas, suggesting that Mmp13 expressed by foamy macrophages may regulate cell–cell interaction or tissue remodeling. Taken together, these identified molecules are involved in the development of necrotizing granulomas through the regulation of foamy macrophage differentiation, localization, and function.

In conclusion, we conducted an in-depth single-cell transcriptomic analysis of necrotizing granulomatous lesions using a TB mouse model that closely recapitulates the pathological features observed in TB patients. Our results revealed novel cellular signatures within necrotizing granulomas, with particular emphasis on the characterization of foamy macrophage. These insights into the cellular and molecular landscape of necrotizing granulomas advance our understanding of TB pathogenesis and will facilitate the development of novel diagnostic tool and host-directed therapeutic drugs for TB.

Materials and methods

Ethics statement

All animal experiments in this study were approved by the Animal Care and Use Committee of The Research Institute of Tuberculosis (RIT) (permission number ID 2022-02) and conducted in accordance with the RIT ethical guidelines for animal care and use.

Mouse model and infection

C3HeB/FeJ mice were purchased from Jackson Laboratory and housed in a filtered-air, laminar-flow cabinet under specific pathogen-free conditions at the animal facility of the RIT. Mice were provided with sterile bedding, water, and mouse chow. Specific pathogen-free status was verified by monitoring sentinel mice housed within the colony. Mice aged 6–10 weeks were transferred to the biosafety level III animal facility of the RIT. For *M. tuberculosis* infection, frozen stocks of the *M. tuberculosis* Erdman strain stored at -80°C was used as previously described (65). Mice were infected with approximately 100 CFU of *M. tuberculosis* bacilli via aerosol using an infection exposure system (Glas-Col).

Preparation of single cells from necrotizing granulomatous lesions

At 12 weeks p.i., infected mice were euthanized by exsanguination under anesthesia with 0.75 mg/kg medetomidine, 4.0 mg/kg midazolam, and 5.0 mg/kg butorphanol via the intraperitoneal route. The lungs were excised and subsequently dissected to collect infected lesions including necrotizing granulomas (Supplementary Figure 1). For the preparation of single-cell suspensions, infected lungs from three or four mice were pooled to collect more than 10 lesions containing necrotizing granulomas. Necrotizing granulomatous lesions were minced and incubated in a collagenase/hyaluronidase/DNase I solution (Stemcell) with RNase inhibitor at 0.2 U/μL. Following red blood cell lysis, the dissociated cells were resuspended in PBS containing 2% fetal bovine serum and RNase inhibitor at 0.2 U/μL. To remove dead cells and a large proportion of neutrophils, cell suspensions were subjected to Ficoll-Paque density gradient centrifugation, followed by the collection of cells from the interface layer according to the manufacturer's instructions (Cytiva).

Construction of scRNA-seq libraries and sequencing

Isolated cell suspensions from necrotizing granulomatous lesions were subjected to scRNA-seq library constructions using Chromium Fixed RNA Profiling Reagent Kit (10x Genomics). Cells were fixed with a fixation solution containing formaldehyde for 24 h at 4°C. Inactivation of *M. tuberculosis* in the fixed samples was confirmed by CFU assay. Fixed cells were further processed to construct scRNA-seq libraries according to the manufacturer's protocol. The resulting libraries were sequenced on NextSeq 1000 (Illumina).

Data analysis

Raw sequencing reads were aligned against the mouse reference genome (mm10) using Cellranger version 7.0.1 (10x Genomics). Subsequent analyses were performed in R version 4.4.1 using the Seurat package version 5.2.1 (66). Data from four independent samples were filtered to include cells with 500–6000 genes and less than 20% mitochondrial reads. Data were normalized using the NormalizeData function, followed by the identification of highly variable features using the FindVariableFeatures function with the variance stabilizing transformation method, selecting the top 2000 most variable genes. Principal component analysis (PCA) was performed using the RunPCA function. To correct for batch effects, the Harmony algorithm was applied using the RunHarmony function. Following batch correction, uniform manifold approximation and projection (UMAP) was computed using the first 30 dimensions. A shared nearest neighbor (SNN) graph was then constructed using the FindNeighbors function with the same set of dimensions. Clustering was performed using the FindClusters function with a resolution parameter set to 0.7. The resulting dataset was processed with scDblFinder version 1.18.0 (67) to remove doublet cells. The filtrated data were reprocessed through data scaling, PCA, UMAP, followed by the construction of SNN graph and clustering. Cell clusters were manually annotated based on specific gene expression patterns of the respective cell types.

Differential expression analysis was performed using Seurat FindMarkers function. Gene expression analysis, GO analysis, and GSEA were performed using Nebulosa version 1.14.0 (68), ShinyGO version 0.82 (69), and, fGSEA version 1.30.00 (70), respectively.

Immunohistochemistry and immunofluorescence microscopy

IHC and IFM were performed as previously described (30, 36). Antibodies used in this study are listed in Supplementary Table 2. IHC and IFM samples were visualized using a NanoZoomer S60 (Hamamatsu Photonics) and a FV4000 (Evident), respectively.

Data availability statement

The datasets presented in this study can be found in online repositories. The names of the repository/repositories and accession number(s) can be found below: https://ddbj.nig.ac.jp/search/entry/bioproject/PRJDB20543. https://ddbj.nig.ac.jp/public/ddbj_database/gea/experiment/E-GEAD-1000/E-GEAD-1082/.

Ethics statement

The animal study was approved by the Animal Care and Use Committee of The Research Institute of Tuberculosis (permission number ID 2022-02). The study was conducted in accordance with the local legislation and institutional requirements.

Author contributions

SS: Funding acquisition, Writing – review & editing, Conceptualization, Writing – original draft, Data curation, Formal Analysis. SO: Writing – review & editing, Methodology. HN: Writing – review & editing, Methodology. MH: Data curation, Conceptualization, Writing – original draft, Funding acquisition, Writing – review & editing, Formal Analysis. NK: Data curation, Conceptualization, Funding acquisition, Formal Analysis, Writing – original draft, Writing – review & editing.

Funding

The author(s) declare that financial support was received for the research and/or publication of this article. This study was supported by the Emerging/Re-emerging Infectious Diseases Project of the Japan Agency for Medical Research and Development (JP23wm0225028, JP23gm1610013, JP23fk0108673, JP23fk0108674, JP23fk0108703, JP25fk0108730), and Grants-in-Aid for Scientific Research, Japan Society for the Promotion of Science (20KK0197, 22K07065).

Acknowledgments

We thank Ms. Miyako Seto and Ms. Mariko Ogasawara in Department of Pathophysiology and Host Defense for technical supports.

Conflict of interest

The authors declare that the research was conducted in the absence of any commercial or financial relationships that could be construed as a potential conflict of interest.

Generative AI statement

The author(s) declare that no Generative AI was used in the creation of this manuscript.

Publisher's note

Supplementary material

The Supplementary Material for this article can be found online at: https://www.frontiersin.org/articles/10.3389/fimmu.2025.1624072/full#supplementary-material

SUPPLEMENTARY FIGURE 1
Macroscopic image of C3HeB/FeJ mouse lung with necrotizing granulomatous lesions at 12 weeks postinfection (p.i.). Arrowheads indicate necrotizing granulomas. Scale bar, 1 cm.

SUPPLEMENTARY FIGURE 2
Violin plots of transcriptional factors regulating T cell differentiation **(A)**, and markers representing memory or effector type **(B)**, and innate lymphoid cells **(C)**.

SUPPLEMENTARY FIGURE 3
GSEA of macrophage clusters characterized by the expression of *Cxcl10* **(A)**, *Clec4e* **(B)**, *C1qc* **(C)**, *Ighm* **(D)**, *S100a9* **(E)**, and *Siglecf* **(F)**. Significantly enriched hallmarks are depicted, representing both activated and suppressed hallmarks in each cluster compared with other clusters.

SUPPLEMENTARY FIGURE 4
Violin plots displaying the characteristic gene expression in the *Ighm*$^{+}$ cluster **(A)** and the *Siglecf*$^{+}$ cluster **(B)**. Gene expression levels of *Cxcl1* and *Hyal1* in macrophage populations are also shown **(C)**.

SUPPLEMENTARY FIGURE 5
Comparative analysis of macrophage populations between C3HeB/FeJ and *Sp140*-deficient mice. Macrophage populations from this study and the GSE216023 dataset from Kotov et al. (28) were integrated and re-clustered. **(A)** Comparative UMAP plots of macrophage clusters between C3HeB/FeJ (FeJ) and *Sp140*-deficient mice (SP140KO), with designated cluster names. **(B, C)** Violin plots showing expression levels of the indicated genes in macrophage clusters from FeJ and SP140KO.

SUPPLEMENTARY TABLE 1
List of differentially expressed genes of the *Plin2*$^{+}$ cluster in the macrophage population.

SUPPLEMENTARY TABLE 2
List of antibodies for IHC and IFM.

References

1. WHO. Tuberculosis(2025). Available online at: https://www.who.int/news-room/fact-sheets/detail/tuberculosis (Accessed March 14, 2025).

2. Cohen SB, Gern BH, Delahaye JL, Adams KN, Plumlee CR, Winkler JK, et al. Alveolar macrophages provide an early mycobacterium tuberculosis niche and initiate dissemination. *Cell Host Microbe*. (2018) 24:439–46.e4. doi: 10.1016/j.chom.2018.08.001

3. Bussi C, Gutierrez MG. Mycobacterium tuberculosis infection of host cells in space and time. *FEMS Microbiol Rev*. (2019) 43:341–61. doi: 10.1093/femsre/fuz006

4. Pagán AJ, Ramakrishnan L. Immunity and immunopathology in the tuberculous granuloma. *Cold Spring Harbor Perspect Med*. (2014) 5:a018499. doi: 10.1101/cshperspect.a018499

5. Sarathy JP, Dartois V. Caseum: A niche for mycobacterium tuberculosis drug-tolerant persisters. *Clin Microbiol Rev*. (2020) 33:e00159-19. doi: 10.1128/cmr.00159-19

6. Cadena AM, Fortune SM, Flynn JL. Heterogeneity in tuberculosis. *Nat Rev Immunol*. (2017) 17:691–702. doi: 10.1038/nri.2017.69

7. Lenaerts A, Barry CE 3rd, Dartois V. Heterogeneity in tuberculosis pathology, microenvironments and therapeutic responses. *Immunol Rev*. (2015) 264:288–307. doi: 10.1111/imr.12252

8. Russell DG, Cardona PJ, Kim MJ, Allain S, Altare F. Foamy macrophages and the progression of the human tuberculosis granuloma. *Nat Immunol*. (2009) 10:943–8. doi: 10.1038/ni.1781

9. Walter ND, Born SEM, Robertson GT, Reichlen M, Dide-Agossou C, Ektnitphong VA, et al. Mycobacterium tuberculosis precursor Rrna as a measure of treatment-shortening activity of drugs and regimens. *Nat Commun*. (2021) 12:2899. doi: 10.1038/s41467-021-22833-6

10. Carow B, Hauling T, Qian X, Kramnik I, Nilsson M, Rottenberg ME. Spatial and temporal localization of immune transcripts defines hallmarks and diversity in the tuberculosis granuloma. *Nat Commun*. (2019) 10:1823. doi: 10.1038/s41467-019-09816-4

11. Kumar R, Kolloli A, Subbian S, Kaushal D, Shi L, Tyagi S. Imaging the architecture of granulomas induced by mycobacterium tuberculosis infection with single-molecule fluorescence in situ hybridization. *J Immunol (Baltimore Md: 1950)*. (2024) 213:526–37. doi: 10.4049/jimmunol.2300068

12. Magoulopoulou A, Qian X, Pediatama Setiabudiawan T, Marco Salas S, Yokota C, Rottenberg ME, et al. Spatial resolution of mycobacterium tuberculosis bacteria and their surrounding immune environments based on selected key transcripts in mouse lungs. *Front Immunol*. (2022) 13:876321. doi: 10.3389/fimmu.2022.876321

13. Qiu X, Zhong P, Yue L, Li C, Yun Z, Si G, et al. Spatial transcriptomic sequencing reveals immune microenvironment features of mycobacterium tuberculosis granulomas in lung and omentum. *Theranostics*. (2024) 14:6185–201. doi: 10.7150/thno.99038

14. McCaffrey EF, Donato M, Keren L, Chen Z, Delmastro A, Fitzpatrick MB, et al. The immunoregulatory landscape of human tuberculosis granulomas. *Nat Immunol*. (2022) 23:318–29. doi: 10.1038/s41590-021-01121-x

15. Bromley JD, Ganchua SKC, Nyquist SK, Maiello P, Chao M, Borish HJ, et al. Cd4 (+) T cells re-wire granuloma cellularity and regulatory networks to promote immunomodulation following Mtb reinfection. *Immunity*. (2024) 57:2380–98.e6. doi: 10.1016/j.immuni.2024.08.002

16. Cinco IR, Napier EG, Rhoades NS, Davies MH, Allison DB, Kohama SG, et al. Immunological and microbial shifts in the aging rhesus macaque lung during nontuberculous mycobacterial infection. *mBio*. (2024) 15:e0082924. doi: 10.1128/mbio.00829-24

17. Pisu D, Johnston L, Mattila JT, Russell DG. The frequency of Cd38(+) alveolar macrophages correlates with early control of M. Tuberculosis in the murine lung. *Nat Commun*. (2024) 15:8522. doi: 10.1038/s41467-024-52846-w

18. Carow B, Muliadi V, Skålén K, Yokota C, Kathamuthu GR, Setiabudiawan TP, et al. Immune mapping of human tuberculosis and sarcoidosis lung granulomas. *Front Immunol*. (2023) 14:1332733. doi: 10.3389/fimmu.2023.1332733

19. Zheng W, Borja M, Dorman LC, Liu J, Zhou A, Seng A, et al. Single-cell analysis reveals mycobacterium tuberculosis esx-1-mediated accumulation of permissive macrophages in infected mouse lungs. *Sci Adv*. (2025) 11:eadq8158. doi: 10.1126/sciadv.adq8158

20. Yang Q, Qi F, Ye T, Li J, Xu G, He X, et al. The interaction of macrophages and cd8 T cells in bronchoalveolar lavage fluid is associated with latent tuberculosis infection. *Emerging Microbes infections*. (2023) 12:2239940. doi: 10.1080/22221751.2023.2239940

21. Winchell CG, Nyquist SK, Chao MC, Maiello P, Myers AJ, Hopkins F, et al. Cd8 + Lymphocytes are critical for early control of tuberculosis in macaques. *J Exp Med*. (2023) 220:e20230707. doi: 10.1084/jem.20230707

22. Wen Z, Wang L, Ma H, Li L, Wan L, Shi L, et al. Integrated single-cell transcriptome and T cell receptor profiling reveals defects of T cell exhaustion in pulmonary tuberculosis. *J infection*. (2024) 88:106158. doi: 10.1016/j.jinf.2024.106158

23. Pisu D, Huang L, Narang V, Theriault M, Lê-Bury G, Lee B, et al. Single cell analysis of M. Tuberculosis phenotype and macrophage lineages in the infected lung. *J Exp Med*. (2021) 218:e20210615. doi: 10.1084/jem.20210615

24. Wang L, Ma H, Wen Z, Niu L, Chen X, Liu H, et al. Single-cell rna-sequencing reveals heterogeneity and intercellular crosstalk in human tuberculosis lung. *J infection*. (2023) 87:373–84. doi: 10.1016/j.jinf.2023.09.004

25. Gideon HP, Hughes TK, Tzouanas CN, Wadsworth MH 2nd, Tu AA, Gierahn TM, et al. Multimodal profiling of lung granulomas in macaques reveals cellular correlates of tuberculosis control. *Immunity*. (2022) 55:827–46.e10. doi: 10.1016/j.immuni.2022.04.004

26. Akter S, Chauhan KS, Dunlap MD, Choreño-Parra JA, Lu L, Esaulova E, et al. Mycobacterium tuberculosis infection drives a type I Ifn signature in lung lymphocytes. *Cell Rep*. (2022) 39:110983. doi: 10.1016/j.celrep.2022.110983

27. Esaulova E, Das S, Singh DK, Choreño-Parra JA, Swain A, Arthur L, et al. The immune landscape in tuberculosis reveals populations linked to disease and latency. *Cell Host Microbe*. (2021) 29:165–78.e8. doi: 10.1016/j.chom.2020.11.013

28. Kotov DI, Lee OV, Fattinger SA, Langner CA, Guillen JV, Peters JM, et al. Early cellular mechanisms of type I interferon-driven susceptibility to tuberculosis. *Cell*. (2023) 186:5536–53.e22. doi: 10.1016/j.cell.2023.11.002

29. Kim MJ, Wainwright HC, Locketz M, Bekker LG, Walther GB, Dittrich C, et al. Caseation of human tuberculosis granulomas correlates with elevated host lipid metabolism. *EMBO Mol Med*. (2010) 2:258–74. doi: 10.1002/emmm.201000079

30. Seto S, Nakamura H, Guo TC, Hikichi H, Wakabayashi K, Miyabayashi A, et al. Spatial multiomic profiling reveals the novel polarization of foamy macrophages within necrotic granulomatous lesions developed in lungs of C3heb/Fej mice infected with mycobacterium tuberculosis. *Front Cell infection Microbiol*. (2022) 12:968543. doi: 10.3389/fcimb.2022.968543

31. Driver ER, Ryan GJ, Hoff DR, Irwin SM, Basaraba RJ, Kramnik I, et al. Evaluation of a mouse model of necrotic granuloma formation using C3heb/Fej mice for testing of drugs against mycobacterium tuberculosis. *Antimicrobial Agents chemotherapy*. (2012) 56:3181–95. doi: 10.1128/aac.00217-12

32. Harper J, Skerry C, Davis SL, Tasneen R, Weir M, Kramnik I, et al. Mouse model of necrotic tuberculosis granulomas develops hypoxic lesions. *J Infect Dis*. (2012) 205:595–602. doi: 10.1093/infdis/jir786

33. Irwin SM, Driver E, Lyon E, Schrupp C, Ryan G, Gonzalez-Juarrero M, et al. Presence of multiple lesion types with vastly different microenvironments in C3heb/Fej mice following aerosol infection with mycobacterium tuberculosis. *Dis Models Mech*. (2015) 8:591–602. doi: 10.1242/dmm.019570

34. Lanoix JP, Lenaerts AJ, Nuermberger EL. Heterogeneous disease progression and treatment response in a C3heb/Fej mouse model of tuberculosis. *Dis Models Mech*. (2015) 8:603–10. doi: 10.1242/dmm.019513

35. Chowdhury CS, Kinsella RL, McNehlan ME, Naik SK, Lane DS, Talukdar P, et al. Type I Ifn-mediated net release promotes mycobacterium tuberculosis replication and is associated with granuloma caseation. *Cell Host Microbe*. (2024) 32:2092–111.e7. doi: 10.1016/j.chom.2024.11.008

36. Seto S, Morimoto K, Yoshida T, Hiramatsu M, Hijikata M, Nagata T, et al. Proteomic profiling reveals the architecture of granulomatous lesions caused by tuberculosis and mycobacterium avium complex lung disease. *Front Microbiol*. (2019) 10:3081. doi: 10.3389/fmicb.2019.03081

37. Hu Y, Hu Q, Li Y, Lu L, Xiang Z, Yin Z, et al. Γδ T cells: origin and fate, subsets, diseases and immunotherapy. *Signal transduction targeted Ther*. (2023) 8:434. doi: 10.1038/s41392-023-01653-8

38. Meraviglia S, El Daker S, Dieli F, Martini F, Martino A. Γδ T cells cross-link innate and adaptive immunity in mycobacterium tuberculosis infection. *Clin Dev Immunol*. (2011) 2011:587315. doi: 10.1155/2011/587315

39. Okazaki T, Honjo T. PD-1 and PD-1 ligands: from discovery to clinical application. *Int. Immunol.*. (2007) 19:813–24. doi: 10.1093/intimm/dxm057

40. Misharin AV, Morales-Nebreda L, Mutlu GM, Budinger GR, Perlman H. Flow cytometric analysis of macrophages and dendritic cell subsets in the mouse lung. *Am J Respir Cell Mol Biol*. (2013) 49:503–10. doi: 10.1165/rcmb.2013-0086MA

41. Bafica A, Scanga CA, Serhan C, MaChado F, White S, Sher A, et al. Host control of mycobacterium tuberculosis is regulated by 5-lipoxygenase-dependent lipoxin production. *J Clin Invest*. (2005) 115:1601–6. doi: 10.1172/jci23949

42. Marakalala MJ, Martinez FO, Plüddemann A, Gordon S. Macrophage heterogeneity in the immunopathogenesis of tuberculosis. *Front Microbiol*. (2018) 9:1028. doi: 10.3389/fmicb.2018.01028

43. Iizasa E, Chuma Y, Uematsu T, Kubota M, Kawaguchi H, Umemura M, et al. Trem2 is a receptor for non-glycosylated mycolic acids of mycobacteria that limits anti-mycobacterial macrophage activation. *Nat Commun*. (2021) 12:2299. doi: 10.1038/s41467-021-22620-3

44. Bogdan C. Nitric oxide synthase in innate and adaptive immunity: an update. *Trends Immunol*. (2015) 36:161–78. doi: 10.1016/j.it.2015.01.003

45. Murray PJ, Allen JE, Biswas SK, Fisher EA, Gilroy DW, Goerdt S, et al. Macrophage activation and polarization: nomenclature and experimental guidelines. *Immunity*. (2014) 41:14–20. doi: 10.1016/j.immuni.2014.06.008

46. Qing F, Liu Z. Interferon regulatory factor 7 in inflammation, cancer and infection. *Front Immunol*. (2023) 14:1190841. doi: 10.3389/fimmu.2023.1190841

47. Hannemann N, Cao S, Eriksson D, Schnelzer A, Jordan J, Eberhardt M, et al. Transcription factor fra-1 targets arginase-1 to enhance macrophage-mediated inflammation in arthritis. *J Clin Invest*. (2019) 129:2669–84. doi: 10.1172/jci96832

48. Nakamura H, Hikichi H, Seto S, Hijikata M, Keicho N. Transcriptional regulators Sp110 and Sp140 modulate inflammatory response genes in mycobacterium tuberculosis-infected human macrophages. *Microbiol Spectr*. (2024) 12:e0010124. doi: 10.1128/spectrum.00101-24

49. Kramnik I, Dietrich WF, Demant P, Bloom BR. Genetic control of resistance to experimental infection with virulent mycobacterium tuberculosis. *Proc Natl Acad Sci United States America*. (2000) 97:8560–5. doi: 10.1073/pnas.150227197

50. Pan H, Yan BS, Rojas M, Shebzukhov YV, Zhou H, Kobzik L, et al. Ipr1 gene mediates innate immunity to tuberculosis. *Nature*. (2005) 434:767–72. doi: 10.1038/nature03419

51. Ji DX, Witt KC, Kotov DI, Margolis SR, Louie A, Chevée V, et al. Role of the transcriptional regulator Sp140 in resistance to bacterial infections via repression of type I interferons. *eLife*. (2021) 10:e67290. doi: 10.7554/eLife.67290

52. Moreira-Teixeira L, Stimpson PJ, Stavropoulos E, Hadebe S, Chakravarty P, Ioannou M, et al. Type I ifn exacerbates disease in tuberculosis-susceptible mice by inducing neutrophil-mediated lung inflammation and netosis. *Nat Commun*. (2020) 11:5566. doi: 10.1038/s41467-020-19412-6

53. Ngo C, Garrec C, Tomasello E, Dalod M. The role of plasmacytoid dendritic cells (Pdcs) in immunity during viral infections and beyond. *Cell Mol Immunol*. (2024) 21:1008–35. doi: 10.1038/s41423-024-01167-5

54. Lee AM, Laurent P, Nathan CF, Barrat FJ. Neutrophil-plasmacytoid dendritic cell interaction leads to production of type I Ifn in response to mycobacterium tuberculosis. *Eur J Immunol*. (2024) 54:e2350666. doi: 10.1002/eji.202350666

55. Guillonneau C, Bézie S, Anegon I. Immunoregulatory properties of the cytokine Il-34. *Cell Mol Life sciences: CMLS*. (2017) 74:2569–86. doi: 10.1007/s00018-017-2482-4

56. Cervenka I, Agudelo LZ, Ruas JL. Kynurenines: tryptophan's metabolites in exercise, inflammation, and mental health. *Sci (New York NY)*. (2017) 357:eaaf9794. doi: 10.1126/science.aaf9794

57. Pan J, Chang Z, Zhang X, Dong Q, Zhao H, Shi J, et al. Research progress of single-cell sequencing in tuberculosis. *Front Immunol*. (2023) 14:1276194. doi: 10.3389/fimmu.2023.1276194

58. Sakai S, Mayer-Barber KD, Barber DL. Defining features of protective Cd4 T cell responses to mycobacterium tuberculosis. *Curr Opin Immunol*. (2014) 29:137–42. doi: 10.1016/j.coi.2014.06.003

59. Torrado E, Cooper AM. Il-17 and Th17 cells in tuberculosis. *Cytokine Growth factor Rev*. (2010) 21:455–62. doi: 10.1016/j.cytogfr.2010.10.004

60. Leane CM, Sutton CE, Moran B, Mills KHG. Pd-1 regulation of pathogenic Il-17-secreting Γδ T cells in experimental autoimmune encephalomyelitis. *Eur J Immunol*. (2024) 54:e2451212. doi: 10.1002/eji.202451212

61. Fang Y, Ma K, Huang YM, Dang Y, Liu Z, Xu Y, et al. Fibronectin leucine-rich transmembrane protein 2 drives monocyte differentiation into macrophages via the Unc5b-Akt/Mtor axis. *Front Immunol*. (2023) 14:1162004. doi: 10.3389/fimmu.2023.1162004

62. Guerrini V, Prideaux B, Blanc L, Bruiners N, Arrigucci R, Singh S, et al. Storage lipid studies in tuberculosis reveal that foam cell biogenesis is disease-specific. *PloS Pathog*. (2018) 14:e1007223. doi: 10.1371/journal.ppat.1007223

63. Martin DC, Atmuri V, Hemming RJ, Farley J, Mort JS, Byers S, et al. A mouse model of human mucopolysaccharidosis ix exhibits osteoarthritis. *Hum Mol Genet*. (2008) 17:1904–15. doi: 10.1093/hmg/ddn088

64. Lee HS, Noh JY, Shin OS, Song JY, Cheong HJ, Kim WJ. Matrix metalloproteinase-13 in atherosclerotic plaque is increased by influenza a virus infection. *J Infect Dis*. (2020) 221:256–66. doi: 10.1093/infdis/jiz580

65. Hikichi H, Seto S, Wakabayashi K, Hijikata M, Keicho N. Transcription factor Mafb controls type I and ii interferon response-mediated host immunity in mycobacterium tuberculosis-infected macrophages. *Front Microbiol*. (2022) 13:962306. doi: 10.3389/fmicb.2022.962306

66. Hao Y, Stuart T, Kowalski MH, Choudhary S, Hoffman P, Hartman A, et al. Dictionary learning for integrative, multimodal and scalable single-cell analysis. *Nat Biotechnol*. (2024) 42:293–304. doi: 10.1038/s41587-023-01767-y

67. Germain PL, Lun A, Garcia Meixide C, Macnair W, Robinson MD. Doublet identification in single-cell sequencing data using Scdblfinder. *F1000Research*. (2021) 10:979. doi: 10.12688/f1000research.73600.2

68. Alquicira-Hernandez J, Powell JE. Nebulosa recovers single-cell gene expression signals by kernel density estimation. *Bioinf (Oxford England)*. (2021) 37:2485–7. doi: 10.1093/bioinformatics/btab003

69. Ge SX, Jung D, Yao R. Shinygo: A graphical gene-set enrichment tool for animals and plants. *Bioinf (Oxford England)*. (2020) 36:2628–9. doi: 10.1093/bioinformatics/btz931

70. Korotkevich G, Sukhov V, Budin N, Shpak B, Artyomov MN, Sergushichev A. Fast gene set enrichment analysis. *bioRxiv*. (2016). doi: 10.1101/060012